A flexibility based beam-column element capable of shear-flexure interaction

M. Sürmeli
Istanbul Kültür University Department of Civil Engineering, Istanbul, Turkey

E. Yüksel
Istanbul Technical University Faculty of Civil Engineering, Istanbul, Turkey

15 WCEE
LISBOA 2012

SUMMARY:
It is essential to employ accurate capacity curve in the performance based design to reach more reliable results on the seismic assessment of reinforced concrete structures. However, the response of shear vulnerable members such as shear wall, spandrel beams, short columns etc. are diverse from those of ductile flexural members. An analytical study is accomplished to account the shear behavior of the members correctly in the existing computer program of DOC3D by means of the newly developed beam-column element. The new flexibility based beam-column element capable of flexure-shear interaction accounting geometrical and material nonlinearity is presented. It is based on cantilever type base element and employs distributed plasticity. The end flexibility terms are determined by summing rotational and transversal deflection differences between successive points by using the developed recurrence relations. Shear-flexure interaction used in the beam-column element is based on the study of Mergos and Kappos (2008) in which an empirical relationship is proposed for evaluating the average shear distortion of reinforced concrete columns at the onset of stirrup yielding. The proposed beam-column element is validated via the envelopes of the experimental results involving reinforced concrete columns subjected to cyclic loading.

Keywords: Shear-flexure interaction, beam column element

1. INTRODUCTION

Past devastating earthquakes showed that old reinforced concrete buildings built without ductile design requirements and/or low concrete compressive strength were collapsed or heavily damaged. The most dangerous collapse mechanism is related to shear which occurs sudden without flexural yielding because of insufficient shear strength. The previous experimental studies exhibited that shear span ratio (α_s=L_s/h), which is defined as the ratio of shear span to column depth for a cantilever column, is the main indicative for the failure type. Shear failure mode is dominated when $\alpha_s < 2.5$ and the member is classified as short column. If α_s increases from 2.5 to 5, the flexure-shear interaction is observed. Greater values of α_s correspond to flexural type failure mode (Ceresa et al., 2008).

The evaluation of existing building's performance under seismic loads is still achieved typically by accounting only flexural type response of the members. The shear-flexural interaction might be imported for some sorts of elements such as short columns or shear vulnerable members. To represent shear-flexural interaction, Guner and Vecchio (2010) were developed an analysis procedure using distributed stress field model (Vecchio and Collins 2000) inherently and accurately account for shear related effects coupled with axial and flexural mechanisms in nonlinear frame behavior. The flexure-shear interaction is a popular subject among researchers in recent years. Xu and Zhang (2011) presented a hysteretic model consists of a flexure and a shear spring coupled at element level in which shear-flexure interaction is considered both at section and element level. Ceresa et al. (2008) developed a flexure-shear model for seismic analysis of RC framed structures according to the Modified Compression Field Theory (Vecchio and Collins, 1986). An enhanced fiber stiffness based element is formulated by Martinelli (2008) to model the effects of shear-flexure interaction in reinforced concrete elements subjected to cycling loading.

In this study, a beam-column element is introduced to be account for both flexural and shear deformations within spread plasticity based on the Timoshenko Beam Theory. In this context, the cantilever type base element is divided into meshes and bending and shear rigidities are updated at the middle of each sub-element. The flexibility terms are determined by summing rotational and transversal displacement differences between successive points by using the developed recurrence relations, Yuksel (1998) and Yuksel and Karadogan (2009). The geometric type nonlinearity is taken into consideration in the element level. Shear-flexure interaction used in the beam-column element is based on the studies of Mergos and Kappos (2008, 2010) in which an empirical relationship is proposed for evaluating the average shear distortion of reinforced concrete columns at the onset of stirrup yielding.

The proposed beam-column element is validated against the envelopes of the experimental results of reinforced concrete columns subjected to cyclic loading.

2. BEAM COLUMN ELEMENT

To analyze nonlinear response of the structures consisting of beam-column elements, a new flexibility based beam column element is presented. The improved primary element accounts for both flexural and shear responses and their interaction. The mathematical model of beam-column element is based on Timoshenko Beam Theory in which plane sections remain plane but neutral axis does not perpendicular to section.

The cantilever type base element with the unknowns (X_1 and X_2) at right end is demonstrated in Fig. 2.1. The length of the element is L and the general load arrangement is distributed.

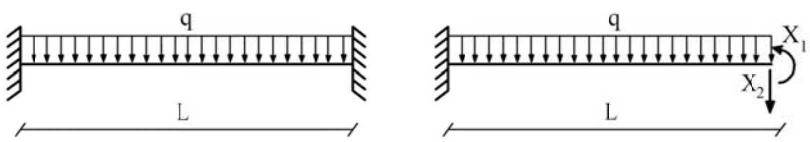

Figure 2.1. Beam-Column Element and the flexibility terms

To consider the spread plasticity through the base element, the beam-column element is divided into m segments whose lengths are $\Delta L=L/m$ (Fig.2.2). The nth segment has three coordinates defined as left, middle and right points (Xl_n, Xm_n and Xr_n) and has flexural and shear rigidities of EI_n and GF_n which are identified at the mid of the segment.

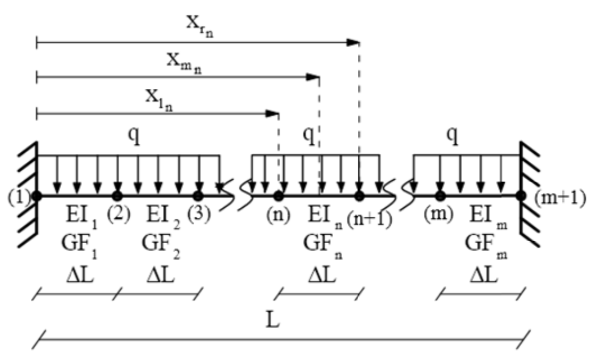

Figure 2.2. Meshed base element

2.1. Flexibility Terms

The flexibility terms identified as f_{ij} is determined by summing rotational and transversal displacement differences calculated for sequential segments from virtual work principle. In the definition of f_{ij}, subscript i define deformation of i^{th} freedom and subscript j stands for the load condition causing the deformation. In this context, $X_1=1$ case is used to determine the flexibility terms of f_{11} and f_{21}; $X_2=1$ case is used to determine the flexibility terms of f_{12} and $f_{22;}$ and distributed load exposed to system yields the flexibility terms of f_{10} and f_{20}. General integral equations of virtual work principle are given below:

$$f_{1j} = \int_0^L \frac{M_j(x) \cdot \bar{M}_\theta(x)}{EI(x)} dx + \int_0^L \frac{T_j(x) \cdot \bar{T}_\theta(x)}{GF'(x)} dx \tag{2.1}$$

$$f_{2j} = \int_0^L \frac{M_j(x) \cdot \bar{M}_\Delta(x)}{EI(x)} dx + \int_0^L \frac{T_j(x) \cdot \bar{T}_\Delta(x)}{GF'(x)} dx \tag{2.2}$$

where, $\bar{M}_\theta$ and $\bar{M}_\Delta$ are virtual moment diagrams, $\bar{T}_\theta$ and $\bar{T}_\Delta$ are virtual shear diagrams to be used in the calculation of rotation and transversal displacement at the right points, Fig.2.3. Moment diagram M_j and shear diagram T_j are associated with the j^{th} load condition. To account geometric nonlinearity, the moment and shear diagrams are updated in each load step till the flexibility terms approach a unique value between the successive steps. If one converts above integral equations into discrete parts, the flexibility terms can be defined as the sum of rotational and transversal displacement differences as given below:

$$f_{1j} = \sum_{i=1}^{m} \Delta\theta_{ij} \qquad\qquad f_{2j} = \sum_{i=1}^{m} \Delta\delta_{ij} \tag{2.3}$$

where, $\Delta\theta_{ij}$ and $\Delta\delta_{ij}$ are the rotational and transversal displacement differences at i^{th} mesh for j^{th} loading condition. In order to calculate $\Delta\theta_{ij}$, unit moments exposed to boundaries of i^{th} mesh; if $\Delta\delta_{ij}$ is required, unit forces at opposite directions should be applied to the boundaries as shown in Fig. 2.3.

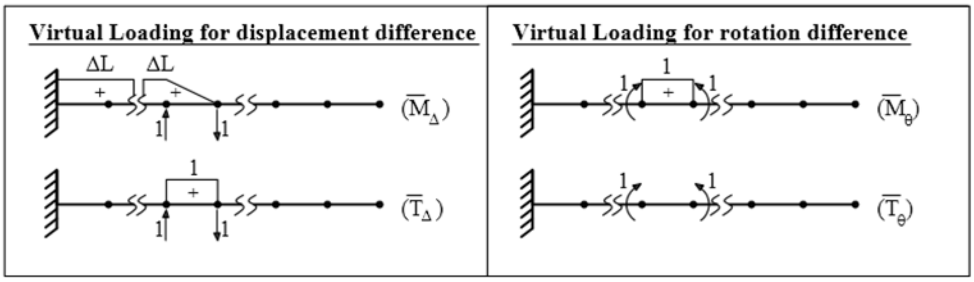

Figure 2.3. Virtual force and moment-shear diagrams for calculating rotation and displacement differences

The application of the load conditions are revealed in Fig. 2.4. As seen from the figure, the moment and shear diagrams M_j and T_j $(j=0,1,2)$ is divided into 1^{st} and 2^{nd} order counterparts by $M_j = M_{0j} + M_{pj}$ and $T_j = T_{0j} + T_{pj}$. The moment and shear diagrams M_{0j}, T_{0j} correspond to 1st order analysis, while M_{pj} and T_{pj} correspond to geometric nonlinearity.

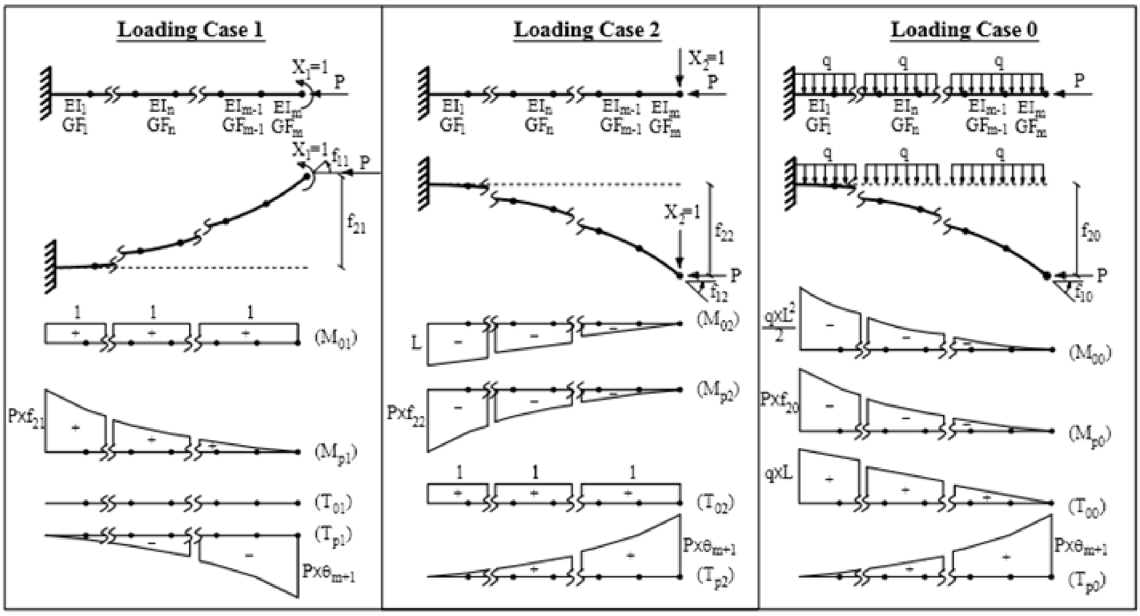

Figure 2.4. Moment and shear diagrams for different loading cases

Once the diagrams are formed, the moments and shears are vectored for each loading condition *(j=0,1,2)* at *(m+1)* nodes as given below:

$$M_j=\begin{bmatrix} M_{j_{(1)}} \\ M_{j_{(2)}} \\ \dots \\ M_{j_{(n)}} \\ \dots \\ M_{j_{(m+1)}} \end{bmatrix} \qquad T_j=\begin{bmatrix} T_{j_{(1)}} \\ T_{j_{(2)}} \\ \dots \\ T_{j_{(n)}} \\ \dots \\ T_{j_{(m+1)}} \end{bmatrix} \tag{2.4}$$

The flexibility term f_{ij} consists of 2nd order flexural and shear responses, hence $f_{ij}=f_{ij\_M}+f_{ij\_T}$. Where, f_{ij_M} is the contribution of flexural responses, while f_{ij_T} corresponds to shear counterpart. The flexural flexibility terms are listed in Table 2.1.

Table 2.1. Flexural flexibility terms

$f_{11\_M}=\sum_{i=1}^{m}\frac{\left(M_{1(i)}+M_{1(i+1)}\right)\Delta L}{2EI_i}$	$f_{21\_M}=\sum_{i=1}^{m}\left[-\frac{\left(2M_{1(i)}+M_{1(i+1)}\right)\Delta L^2}{6EI_i}-\sum_{j=2}^{i\ge2}\frac{\left(M_{1(j-1)}+M_{1(j)}\right)\Delta L^2}{2EI_{j-1}}\right]$
$f_{12\_M}=\sum_{i=1}^{m}\left[\frac{\left(M_{2(i)}+M_{2(i+1)}\right)\Delta L}{2EI_i}\right]$	$f_{22\_M}=\sum_{i=1}^{m}\left[-\frac{\left(2M_{2(i)}+M_{2(i+1)}\right)\Delta L^2}{6EI_i}-\sum_{j=2}^{i\ge2}\frac{\left(M_{2(j-1)}+M_{2(j)}\right)\Delta L^2}{2EI_{j-1}}\right]$
$f_{10\_M}=\sum_{i=1}^{m}\frac{q}{EI_i}\cdot\left(-L^2\cdot\frac{\Delta L}{2}+L\cdot\Delta L\cdot x_{m(i)}-\frac{\left(x_{r(i)}^3-x_{l(i)}^3\right)}{6}+\frac{\left(M_{P0(i)}+M_{P0(i+1)}\right)\Delta L}{2EI_i}\right)$	
$f_{20\_M}=\sum_{i=1}^{m}\left[\frac{q}{EI_i}\left(\frac{(L\cdot\Delta L)^2}{4}-L\cdot\Delta L\cdot x_{m(i)}\cdot x_{r(i)}+\left(x_{r(i)}^3-x_{l(i)}^3\right)\cdot\left(\frac{L}{3}+\frac{x_{r(i)}}{6}\right)-\frac{\left(x_{r(i)}^4-x_{l(i)}^4\right)}{8}\right)+\sum_{j=2}^{i\ge2}\frac{q\cdot\Delta L}{EI_{j-1}}\left(L^2\cdot\frac{\Delta L}{2}-L\cdot\Delta L\cdot x_{m(j-1)}+\frac{x_{r(j-1)}^3-x_{l(j-1)}^3}{6}-\frac{\left(M_{P0(j-1)}+M_{P0(j)}\right)\Delta L^2}{2EI_{j-1}}\right)-\frac{\left(2M_{P0(i)}+M_{P0(i+1)}\right)\Delta L^2}{6EI_i}\right]$	

The flexibility terms related to shear are listed in Table 2.2.

Table 2.2. Flexural terms related to shear

$f_{11\_T}=\sum_{i=1}^{m}\frac{P\cdot\Delta\theta_{i1}}{GF_i}$	$f_{21\_T}=\sum_{i=1}^{m}\frac{P\cdot\Delta\delta_{i1}}{GF_i}$	$f_{12\_T}=\sum_{i=1}^{m}\frac{P\cdot\Delta\theta_{i2}}{GF_i}$
$f_{22\_T}=\sum_{i=1}^{m}\frac{\Delta L+P\cdot\Delta\delta_{i2}}{GF_i}$	$f_{10\_T}=\sum_{i=1}^{m}\frac{P\cdot\Delta\theta_{i0}-q\cdot\Delta L}{GF_i}$	$f_{20\_T}=\sum_{i=1}^{m}\left[\frac{q\cdot\Delta L\cdot\left(L-x_{ort(i)}\right)+P\cdot\Delta\delta_{i0}}{GF_i}\right]$

2.2. ELEMENT RIGIDITY MATRIX

Once flexibility matrix [*f*] is attained, stiffness matrix is calculated as follows:

$$[f]=\begin{bmatrix} f_{11} & f_{12} \\ f_{21} & f_{22} \end{bmatrix} \qquad \left[\bar{k}\right]=\begin{bmatrix} \bar{k}_{11} & \bar{k}_{12} \\ \bar{k}_{21} & \bar{k}_{22} \end{bmatrix}=[f]^{-1} \tag{2.5}$$

The complete element stiffness matrix is obtained by using the equilibrium equations on the beam-column element, Fig. 2.5.

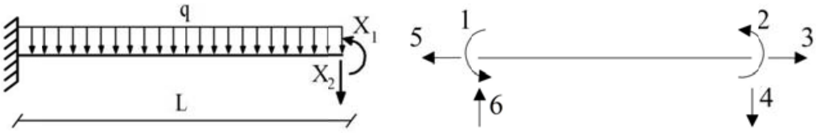

Figure 2.5. The degree of freedoms of local axis system

3. MATERIAL NONLINEARITY

The moment-curvature relations are created by an improved sectional analysis program. The program can take into account Mander unconfined-confined concrete models (Mander et al. 1988) and bilinear-parabolic strain hardening model. Once the moment curvature relation is obtained, linearization procedure using secant stiffness is employed as shown in Fig. 3.1.

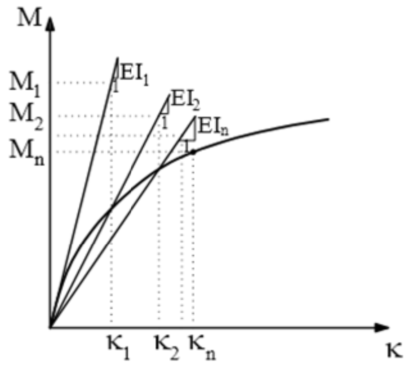

Figure 3.1. Secant stiffness method

Shear-flexure interaction used in the beam-column element is based on the studies of Mergos and Kappos (2008, 2010). According to these studies, shear force-shear distortion envelope is created due to current curvature ductility demand (μ). If current ductility μ is smaller than 3, there is no interaction between shear and flexure and capacity curve is bilinear with cracking and ultimate points as shown in Fig. 3.2. Whereby, V_{cr}, V_y and V_{u0} corresponds to cracking, flexural yielding and ultimate shear strengths (yielding of transverse reinforcement); γ_{cr}, γ_y and γ_u are related shear distortions, respectively. GA_0 is initial shear stiffness, GA_1 post cracking stiffness for un-degraded case. This is the case when shear response dominates the behavior over flexure such as short beams, link beams, etc. For increasing curvature ductility demands (μ>3), shear strength reduces as shown in the figure on the right. The shear forces $V_{\mu=3}$, $V_{\mu=7}$ and $V_{\mu=15}$ corresponds to ductility demands μ=3, μ=7, μ=15; $\gamma_{\mu=3}$, $\gamma_{\mu=7}$ and $\gamma_{\mu=15}$ are related shear distortions, respectively. If ductility is between 3 and 7, the post-cracking stiffness (GA_1) reduces to GA_2; and for 7<μ<15, GA_1 reduces to GA_3. For other cases post cracking stiffness is equal to GA_1.

The cracking strength is given by Sezen and Moehle (2004) as follows:

$$V_{cr} = \frac{f_{ctm}}{L_s / h}\sqrt{1+\frac{N}{f_{ctm}\cdot A_g}} \times A_0 \tag{3.1}$$

Where, f_{ctm} is the mean concrete tensile strength, N is compressive axial load, L_s/h is shear span ratio and A_g is gross sectional area. G is the elastic shear modulus. A_0=0.8A_g is the effective area to take into account a parabolic shear stress distribution along the depth of the cross section. Then the cracking shear distortion is calculated by $\gamma_{cr} = V_{cr} / GA_0$.

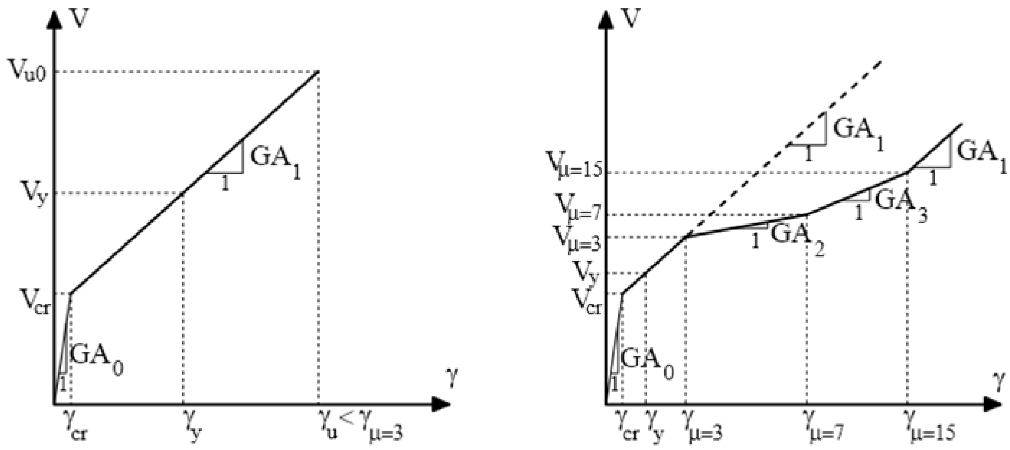

Figure 3.2. Shear distortion-shear force envelopes

The ultimate shear strength is given by Priestley et al. (1994) with the following formula:

$$V_u = k\cdot\sqrt{f_c\cdot\left(0.8A_g\right)} + N\cdot\tan\alpha + \frac{A_w\cdot f_{yw}\cdot\left(d-d'\right)\cot\theta}{s} \tag{3.2}$$

where, f_c concrete compressive strength; A_w is transverse reinforcement area; f_{yw} is transverse reinforcement yield strength; θ is the angle defined by the column axis and the direction of the diagonal compression struts and regression analysis show that it can be taken to be equal to 35°; d - d' is the distance measured parallel to the applied shear between the centers of longitudinal reinforcement; s is spacing of transverse reinforcement; α is the angle between the column axis and the line joining the centers of the flexural compression zones at the top and bottom of the column. The factor k is a parameter depending on the curvature ductility demand as shown in Fig. 3.3.

The ultimate shear distortion is estimated using the truss analogy approach proposed by Park and Paulay (1975) and Kowalsky et al. (1995) and calculated with following formula:

$$\gamma_{uo} = \frac{V_{cr}}{GA_0} + \frac{A_w\cdot f_{yw}\cdot\cot\theta}{s}\cdot\left(\frac{s}{E_s\cdot A_w\cdot\cot\theta^2} + \frac{1}{E_c\cdot b\cdot\sin\theta^3\cdot\cos\theta\cdot\cot\theta}\right) \tag{3.3}$$

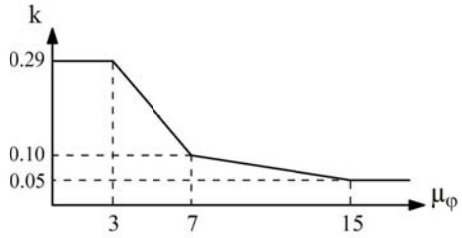

Figure 3.3. k factors

Where, E_s is steel elasticity modulus, E_c is concrete elasticity modulus and b is width of the cross section. Mergos and Kappos (2008) proposed two modification factors to account for axial load and column aspect ratio for deriving ultimate shear distortion. The first modification factor, κ, takes into account the influence of the axial load and is given by:

$$\kappa = 1 - 1.03 \cdot \nu \qquad \nu = N / \left(A_g \cdot f_c \right) \tag{3.4}$$

The second modification factor, λ, represents the influence of the column aspect ratio and is given by the following expression:

$$\lambda = 5.41 - 1.13 \cdot \left(\frac{L_s}{h} \right) \geq 1 \tag{3.5}$$

Then, the resulted ultimate shear distortion is given by:

$$\gamma_u = \kappa \cdot \lambda \cdot \gamma_{uo} \tag{3.6}$$

The implementation of shear-flexure interaction is shown in Fig. 3.4. Herein, the dashed line corresponds to un-degraded case and V_i is the shear force at i^{th} analysis step at which flexural yielding was occurred before. The shear force difference (ΔV) is the difference between V_i and V_{cr}. The term $\Delta degV_c$ is the difference between the V_{u0} and the ultimate shear strength (V_u) derived from the current curvature ductility. Once ΔV and $\Delta degV_c$ are obtained, $\Delta\gamma_i$ and hence effective shear rigidity (GA_{eff}) at the next analysis step can be calculated as Eq. 3.7.

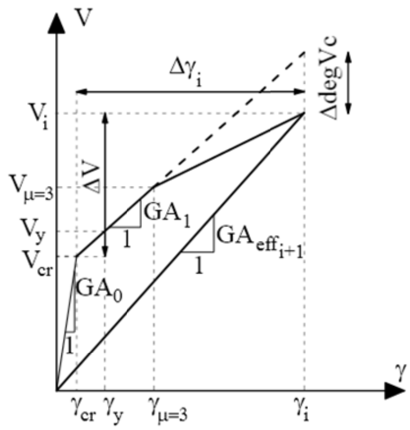

Figure 3.4. Implementation of shear-flexure interaction

$$\Delta\gamma_i = \frac{\Delta V + \Delta \deg V_c}{GA_1} \qquad \mathrm{GA}_{eff_{i+1}} = \frac{V_i}{\gamma_i} \tag{3.7}$$

4. EXPERIMENTAL VERIFICATION

To verify the accuracy of the developed algorithm, two column specimens which were exposed to cyclic loading were used. The first example demonstrates shear-flexure behavior, while the collapse mechanism of the second one is shear.

4.1. Flexure-Shear Critical Example

The flexure-shear critical column example were taken from Lynn et al.(1996). The column has dimensions of 457×457 mm as shown in Fig. 4.1 and has a height of 1473 mm. Hence, the shear span ratio is L_s/h=3.22.

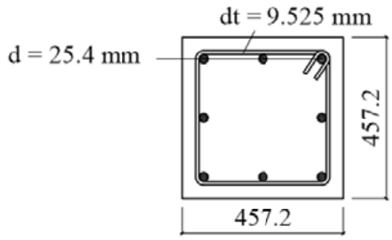

Figure 4.1. The cross section of flexure-shear critical specimen

The axial load is 503 kN which is the 6% of the column compressive strength. The concrete compressive strength is 41 MPa, yield strength of longitudinal reinforcement (f_{yl}) is 331 MPa, the ultimate strength of longitudinal reinforcement is (f_{su}) 496 MPa, the yield strength of transverse reinforcement (f_{yw}) is 400 Mpa. The section consists of eight longitudinal bars having a diameter of 25.4 mm. Diameter of the lateral reinforcement is 9.53 mm.

Two pushover analyses with developed algorithm were performed and the obtained top displacement vs. base shear force relation compared with experimental hysteresis, Fig. 4.2. The red curve corresponds to the analysis in which flexure-shear interaction is considered whereas the black one is the result of the analysis in which only flexural type deformation accounted.

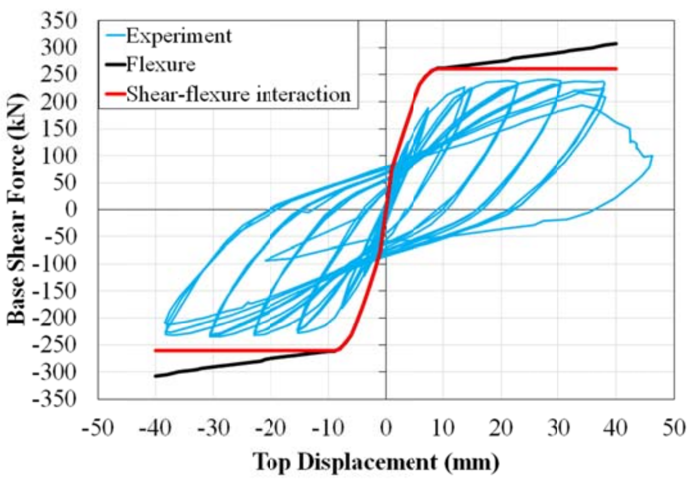

Figure 4.2. The comparison of experiment and numerical results

4.2- Shear Critical Example

The flexure-shear critical column example were taken from Abouteha et al.(1999). The column has dimensions of 457×914 mm as shown in Fig. 4.3 and has a height of 1219 mm. Hence, the shear span ratio is $L_s/h=1.33$.

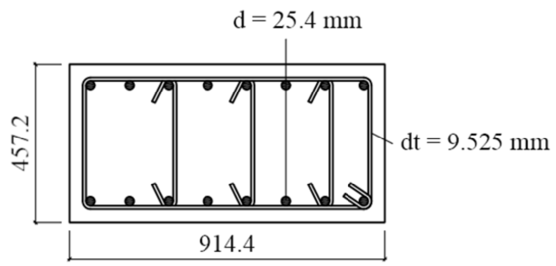

Figure 4.3. The cross section of shear critical specimen

There exists no axial load on the specimen. The concrete compressive strength is 16 MPa, yield strength of longitudinal reinforcement (f_{yl}) is 434 MPa, the ultimate strength of longitudinal reinforcement is (f_{su}) 690 MPa, the yield strength of transverse reinforcement (f_{yw}) is 400 MPa. The section consists of sixteen longitudinal bars having a diameter of 25.4 mm and transversal reinforcement of 9.53 mm in diameter.

Two pushover analyses with developed algorithm were performed and the obtained top displacement vs. base shear force relation is compared with the experimental hysteresis, Fig. 4.4. The red curve is the result of the analysis in which flexure-shear interaction is considered whereas the black one corresponds to the analysis in which only flexural deformation is taken into account.

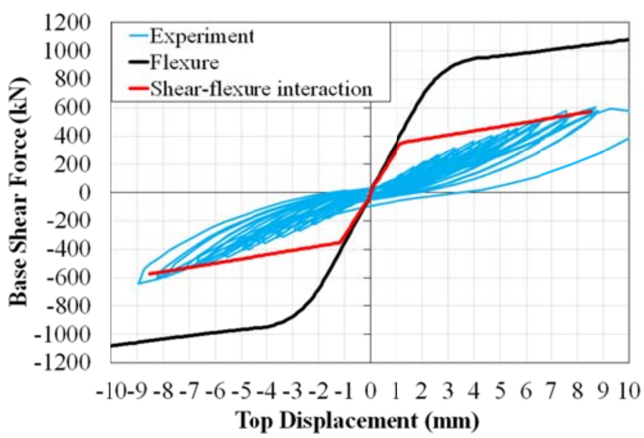

Figure 4.4. The comparison of experiment and numerical results

5. CONCLUSIONS

A flexibility based beam-column element capable of flexure-shear interaction accounting geometrical and material nonlinearity is presented. The proposed beam-column element is validated against the envelopes of the experimental results involving reinforced concrete columns subjected to cyclic loading. The consequence of flexural-shear interaction has been understood clearly in the obtained response curves. In the flexural-shear critical example ($L_s/h=3.22$), the initial stiffness and the ultimate loading capacity are well estimated; there is some gap in pre-yielding stiffness. In the shear critical example ($L_s/h=1.33$), although the ultimate loading capacity are well estimated, there is certain gap in pre-yielding stiffness.

REFERENCES

Aboutaha, R.S., Engelhardt, M.D., Jirsa, J.O., Kreger, M.E. (1999). Rehabilitation of Shear Critical Concrete Columns by Use of Rectangular Steel Jackets. *ACI Structural Journal*. **96**:**1**, 68–78.

Ceresa, P., Petrini, L., Pinho, R. (2008), A Fibre Flexure-Shear Model for Cyclic Nonlinear Behaviour of RC Structural Elements, IUSS, Pavia, Italy.

Guner, S., Vecchio, F.J. (2010). Pushover Analysis of Shear-Critical Frames: Formulation. *ACI Structural Journal.***107:1**, 63-71.

Kowalsky, M.J., Priestley M.J.N., F, Seible. (1995). Shear behaviour of lightweight concrete columns under seismic conditions. Report No. SSRP-95/10, University of California, San Diego, CA.

Lynn, A.C., Moehle, J.P., Mahin, S.A., Holmes, W.T. (1996). Seismic evaluation of existing reinforced concrete building columns. *Earthquake Spectra*. **12:4**, 715–739.

Mander, J.B., Priestley, M.J.N., Park, R. (1988). Theoretical Stress-Strain Model for Confined Concrete. *Journal of Structural Engineering*. **114:8**, 1804-1826.

Martinelli, L. (2008). Modeling Shear-Flexure Interaction in Reinforced Concrete Elements Subjected to Cyclic Lateral Loading. *ACI Structural Journal*. **105:6**, 675-684.

Park, R., Paulay, T. (1975). Reinforced Concrete Structures, Wiley, New York.

P.E., Mergos, A.J., Kappos. (2008). A distributed shear and flexural flexibility model with shear-flexure interaction for R/C members subjected to seismic loading. *Earthquake Engineering and Structural Dynamics*. **37:12**, 1349-1370.

P.E., Mergos, A.J., Kappos. (2010). Seismic damage analysis including inelastic shear-flexure interaction. *Bulletin of Earthquake Engineering*. **8:1**, 27-46.

Priestley, M.J.N., Verma, R., Xiao, Y. (1994). Seismic shear strength of reinforced concrete columns. *Journal of StructuralEngineering*. **120:8**, 2310–2329.

Sezen, H., Moehle, J.P. (2004). Shear strength model for lightly reinforced concrete columns. *Journal of Structural Engineering.* **130:11**, 1692–1703.

Vecchio, F.J., Collins, M.P. (2000). Distributed stress field model for reinforced concrete: Formulation. *Journal of Structural Engineering*, ASCE. **126:9**, 1070-1077.

Vecchio, F.J., Collins, M.P. (1986). The Modified Compression-Field Theory for Reinforced Concrete Elements Subjected to Shear. *ACI Structural Journal*. **83:2**, 219-231.

Xu, S., Zhang, J. (2011). Hysteretic shear-flexure interaction model of reinforced concrete columns for seismic response assessment of bridges. *Earthquake Engineering and Structural Dynamics.* **40**, 315-337.

Yüksel, E. (1998). Nonlinear Analysis of 3D Large Structures with Certain Irregularities, Ph.D. Thesis, submitted to Graduate Scholl of ITU (in Turkish).

Yüksel, E., Karadoğan, F. (2009). Simplified Calculation Approach of Load-Deformation Relationships of a Beam-Column Element. *G.U. Journal of Science*. **22:4**, 341-350.